3D-Printed Scanning-Probe Microscopes with Integrated Optical Actuation and Read-Out

Philipp-Immanuel Dietrich,* Gerald Göring, Mareike Trappen, Matthias Blaicher, Wolfgang Freude, Thomas Schimmel, Hendrik Hölscher,* and Christian Koos*

Scanning-probe microscopy (SPM) is the method of choice for high-resolution imaging of surfaces in science and industry. However, SPM systems are still considered as rather complex and costly scientific instruments, realized by delicate combinations of microscopic cantilevers, nanoscopic tips, and macroscopic read-out units that require high-precision alignment prior to use. This study introduces a concept of ultra-compact SPM engines that combine cantilevers, tips, and a wide variety of actuator and read-out elements into one single monolithic structure. The devices are fabricated by multiphoton laser lithography as it is a particularly flexible and accurate additive nanofabrication technique. The resulting SPM engines are operated by optical actuation and read-out without manual alignment of individual components. The viability of the concept is demonstrated in a series of experiments that range from atomic-force microscopy engines offering atomic step height resolution, their operation in fluids, and to 3D printed scanning near-field optical microscopy. The presented approach is amenable to wafer-scale mass fabrication of SPM arrays and capable to unlock a wide range of novel applications that are inaccessible by current approaches to build SPMs.

1. Introduction

Scanning probe microscopy (SPM)[1] is a widely used tool to analyze and manipulate objects on the nanometer scale, enabling, e.g., surface characterization[2,3] and nanofabrication[4] with atomic resolution, high-density data storage,[5,6] or imaging of biological processes.[7–9] At its heart, SPM relies on interactions of a sample surface with a mechanical probe, commonly

realized as a sharp tip with nanometer-size apex attached to a micrometer-scale cantilever. In current SPM systems, tip and cantilever are usually structured in a dedicated microfabrication process before being manually mounted and aligned to a macroscopic optomechanical system for piezoelectric actuation and optical detection of sub-nanometer movements. This concept leads to rather bulky implementations and requires laborious operation, given that the tip is a wear part that has to be regularly exchanged and re-aligned to the read-out system. In addition, tip-cantilever geometries are currently restricted by the underlying fabrication techniques, relying on 2D lithographic patterning and subsequent anisotropic etching. These techniques usually result in pyramidal tips with rather low aspect ratios, and the dimensions of the cantilever are often subject to fabrication tolerances that lead to variations of the resonance frequency of 30%

or more.[10] Moreover, current SPM systems are often limited in scanning speed, which inhibits high-throughput characterization of large sample areas. This may be overcome by arrays of SPM cantilevers for parallel scanning,[11,12] but the scalability and integration density of current SPM schemes is limited by the fact that each cantilever must still be individually addressed by a dedicated actuator and sensor element of macroscopic dimension. Chip-level integration of individually addressable cantilevers has been

---

P.-I. Dietrich, M. Trappen, M. Blaicher, Prof. H. Hölscher
Prof. C. Koos
Institute for Microstructure Technology (IMT)
Karlsruhe Institute of Technology (KIT)
Hermann-von-Helmholtz-Platz 1, 76344 Eggenstein-Leopoldshafen,
Germany
E-mail: p-i.dietrich@kit.edu; hendrik.hoelscher@kit.edu;
christian.koos@kit.edu

The ORCID identification number(s) for the author(s) of this article can be found under https://doi.org/10.1002/smll.201904695.

P.-I. Dietrich, M. Trappen, M. Blaicher, Prof. W. Freude, Prof. C. Koos
Institute of Photonics and Quantum Electronics (IPQ)
Karlsruhe Institute of Technology (KIT)
Engesserstraße 5, 76131 Karlsruhe, Germany

P.-I. Dietrich, Prof. C. Koos
Vanguard Photonics GmbH
Gablonzer Straße 10, 76185 Karlsruhe, Germany

M. Trappen, Prof. C. Koos
3DMM2O - Cluster of Excellence
(EXC-2082/1 – 390761711)
Karlsruhe Institute of Technology (KIT)
Engesserstraße 5, 76131 Karlsruhe, Germany

Dr. G. Göring, Prof. T. Schimmel
Institute of Applied Physics (APH)
Karlsruhe Institute of Technology (KIT)
Wolfgang-Gaede-Straße 1, 76131 Karlsruhe, Germany

Dr. G. Göring, Prof. T. Schimmel
Institute of Nanotechnology (INT)
Karlsruhe Institute of Technology (KIT)
Hermann-von-Helmholtz-Platz 1, 76344 Eggenstein-Leopoldshafen,
Germany

**ADVANCED
SCIENCE NEWS**
www.advancedsciencenews.com

NANO · MICRO
small
www.small-journal.com

demonstrated in the context of nanomechanical data storage, also known as "millipede memory."[5,6] These experiments resulted in an impressive number of more than 4000 cantilevers realized on a single substrate, but the functionality of each individual cantilever was restricted to creating and detecting indentations in polymer surfaces, corresponding to single-bit writing or reading, rather than allowing for characterization of general topographies. In many applications, it is desirable to complement SPM by additional imaging modes. One of the most prominent examples is scanning near-field optical microscopy (SNOM),[13,14] which is used to measure optical properties with sub-wavelength resolution, e.g., in life sciences[15,16] and material research,[17–19] or for characterization of integrated optical devices.[20,21] SNOM crucially relies on coupling of light to and from a metal nanoscale probe tip and hence requires additional macroscopic optical elements such as microscope objectives or mirrors that need to be precisely aligned. Alternatively, the probe can be realized as metal-coated tip of a tapered optical fiber with a nanoscale aperture at the apex. This concept allows to use the fiber to couple light to and from the probe tip, but relies on elaborate fabrication processes which often involve manual pulling or etching of the fiber tip, followed by delicate coating processes.[22]

Here, we demonstrate that direct-write 3D laser lithography opens new perspectives for fabrication of particularly compact and robust SPM systems that overcome most of the aforementioned limitations. Our approach relies on multiphoton polymerization and allows fabricating monolithic 3D freeform structures that combine cantilevers and tips with additional elements to fully functional SPM engines which are optically actuated and probed. The SPM engines including tips are in situ printed with high precision in a single process directly on facets of optical devices, thus rendering further alignment obsolete. The concept offers vast geometrical design freedom along with highly reproducible fabrication and lends itself to 3D-printing of large-scale SPM arrays with individual actuator and sensor elements. Moreover, additional imaging modes such as SNOM may be implemented by monolithic co-integration of the SPM engines with printed micro-optical freeform components such as lenses and mirrors. We demonstrate the viability of our approach by fabricating SPM engines directly on the facets of optical fiber arrays, which deliver and collect light for remote actuation and probing. These SPM engines offer atomic step-height resolution and are suited for operation both in air and in liquids. We further expand the concept to monolithically integrated SNOM engines, and which enable imaging of optical nanostructures with sub-wavelength resolution. To demonstrate that our approach is also suited for wafer-scale mass fabrication, we print more than 60 nominally identical devices and confirm their reproducibility. We believe that our experiments pave the route toward additive 3D nanofabrication of a wide variety of highly integrated SPM systems.

2. Concept of 3D-Printed SPM Engines, their Fabrication and Characterization

The concept of a 3D-nanoprinted SPM engine is illustrated in **Figure 1**. The structure is fabricated on the facet of a single-mode fiber (SMF) array through which light is guided to and collected

from the device. A cut-open 3D-model of the printed structure is shown in Figure 1a along with the various light paths (red). For actuation of the depicted structure, light is supplied through SMF1 and redirected by two total-internal reflection (TIR) mirrors to locally heat the metal-coated top surface of the cantilever, thereby inducing thermal expansion. By sinusoidal modulation of the optical power, we excite the cantilever close to its resonance frequency. The position of the cantilever is detected interferometrically through SMF2. Hence, light is emitted from the fiber facet toward a concave freeform mirror MI at the bottom surface of the cantilever, designed for focusing a portion of the light back into the fiber core. Depending on the position of the cantilever, this portion of light interferes constructively or destructively with the Fresnel reflection at the inner fiber facet. By appropriate design of the freeform mirror, the optical amplitude of the back-coupled light can be matched to the Fresnel reflection from the fiber facet, thus ensuring complete extinction of the two partial waves for a relative phase shift of π. Please see Section S3 (Supporting Information) for more details. The cantilever is equipped with a printed probe tip, which can be tailored to the specific application. Fibers SMF3 and SMF4 are used for complementing the SPM engine by SNOM functionality. Thus, the sample area around the probe tip is locally illuminated through SMF4 and a combination of a freeform metal mirror and a freeform lens, which are both printed along with the cantilever and the tip to ensure perfect alignment. For SNOM detection, the tip is equipped with a sub-wavelength metal aperture through, which light is coupled to SMF3 and routed to a photodetector.

A scanning-electron microscope (SEM) image of a fabricated SPM engine is shown in Figure 1b. The cantilever and the optics of the SPM engine were 3D-printed to the SMF array by two-photon laser lithography, see the Experimental Section for more details. Two-photon lithography has previously been used for fabrication of a wide variety of functional structures, comprising, e.g., optical freeform elements at the facets of optical fibers[23,24] and optical single-mode waveguides[25,26] as well as atomic-force microscopy (AFM) tips[27] and cantilevers[28] or read-out optics for scanning-tunneling microscope tips.[29] After 3D printing the main structure, the top surface is covered by a metal coating of 5 nm chromium (Cr) followed by 100 nm gold (Au), the former acting as an absorber for the 785 nm actuation light supplied through SMF1. Dedicated shielding structures prevent unwanted metal coating of mirror and lens surfaces. For SNOM operation, a sub-wavelength aperture is opened at the apex of the tip by scanning across a corrugated metal surface. Please see the Experimental Section and Section S1 (Supporting Information) for more details on the design and fabrication of the SPM and SNOM engines.

To calibrate the position sensor connected to SMF2, we move the fiber array with the SPM engine toward the surface of the sample using a high-precision piezoelectric translation stage while measuring the displacement of the position detector mirror MI (Figure 1c). The vertical position at which the tip touches down on the sample surface defines the zero point of the z-axis; negative values of z correspond to a movement toward the surface leading to a deformation of the cantilever and a movement Δz_M of mirror MI, whereas positive distances lead to a detachment of the tip from the sample surface. If the sample surface is stiff, Δz_M shows a linear z-dependence for

ADVANCED
SCIENCE NEWS
www.advancedsciencenews.com

NANO · MICRO
small
www.small-journal.com

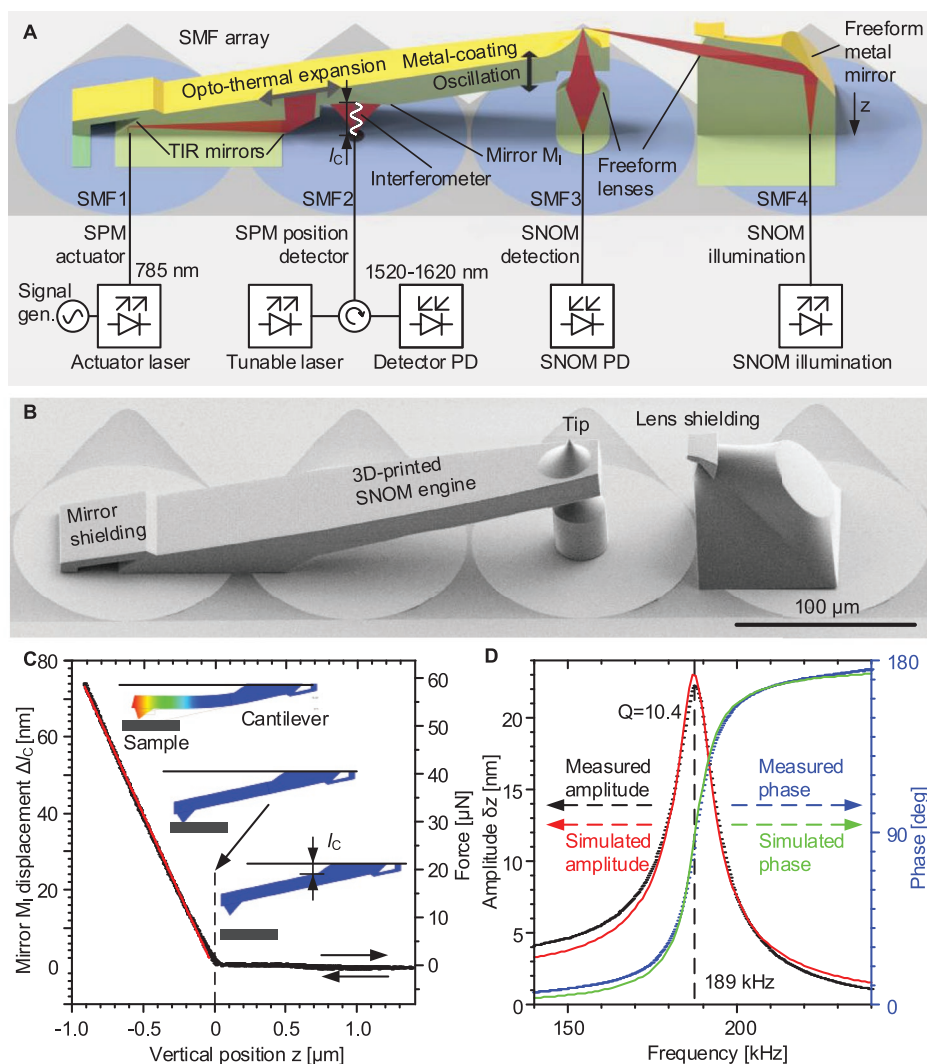**Figure 1.** 3D printing of SPM engines allows to realize large variety of ultra-compact designs. The illustrated device is attached to the facet of a single-mode fiber array and combines an atomic-force microscope and a scanning near-field microscope. Micro-optical elements used for illumination and light collection are printed along with the cantilever and the tip to ensure perfect alignment. A) Schematic drawing of the SPM engine (green) including metal coatings (yellow) and light propagation paths (red). The cantilever is actuated by light supplied through SMF1, which is redirected by two total-internal reflection (TIR) mirrors to locally heat the metal-coated top surface. The position of the cantilever is detected through SMF2 by exploiting the interference of light reflected from a freeform mirror M_I with the Fresnel reflection at the inner surface of the plane fiber facet. SMF4 is used to locally illuminate the sample for SNOM excitation. For detection, the tip is equipped with a sub-wavelength metal aperture through which light is coupled to SMF3. B) SEM image of the SPM engine. Shielding structures prevent unwanted metal coating of lens surfaces. C) Characterization of the AFM position sensor: the AFM engine is moved along the vertical direction (z-direction) toward the sample surface by a high-precision piezoelectric positioner while monitoring the displacement Δz_M of the mirror M_I. Due to a high spring constant of 64 N m^{-1} the curve does not exhibit any jump-to-contact behavior. D) Characterization of the mechanical cantilever resonance: measured (black) and simulated (red) oscillation amplitude δz and measured (blue) and simulated (green) phase of the tip as a function of the power modulation frequency. The phase and the amplitude characteristics exhibit a distinct resonance at a frequency of 189 kHz with a quality factor of 10.4.

$z < 0$ and the measured slope $|\Delta z|/|\Delta z_M| = 13.4$ corresponds to the ratio between the z-displacement $|\Delta z|$ of the probe tip and the z-displacement $|\Delta z_M|$ of the interferometer mirror M_I (Figure S4, Supporting Information). The measured displacement ratio is in good agreement with its simulated value of 13.6 (see Sections S2 and S3 in the Supporting Information for details of the position sensor readout and the simulation technique).

To characterize the dynamic behavior of the cantilever, we sweep the power modulation frequency of the optical actuation signal and continuously measure the oscillation amplitude

of the cantilever using the position detector (Figure 1d). This measurement was conducted with a commercial AFM controller that comprises a signal generator for modulating the actuation power and a lock-in amplifier for read-out of the position detector. The measured phase (blue) and amplitude (black) are in good agreement with simulations (green and red, see Section S4 in the Supporting Information for details). From these measurements, we extracted a resonance frequency of 189 kHz and a quality factor of $Q = 10.4$. Such comparable low quality factors are typical for cantilevers made from polymers and allow for

ADVANCED
SCIENCE NEWS
www.advancedsciencenews.com

NANO · MICRO
small
www.small-journal.com

fast scanning.[30] When exciting the cantilever at its resonance frequency with an optical signal at a wavelength of 785 nm and an optical power modulation amplitude of ≈10 mW, we observe a tip oscillation amplitude of 24 nm, which is sufficient for most applications. Details on the measurement technique can be found in Sections S2 and S3 (Supporting Information). The oscillation amplitude can be controlled by appropriate choice of the power modulation amplitudes or by adapting the mechanical design to provide softer or stiffer cantilevers.

3. Experiments with 3D-Printed SPM Engines

3.1. Atomic Force Microscopy with Atomic Step-Height Resolution

To demonstrate the viability of the concept presented in the previous section, we first test its ability to measure atomic steps. For that we fabricated a simple AFM engine without SNOM functionality as shown in **Figure 2**a, which features a reduced cantilever thickness of 10 μm and a reduced spring constant of $c_{AFM} = 12$ N m^{-1} (Section S2, Supporting Information). In addition, we place the AFM position detector right below the tip to directly extract the tip movement (displacement ratio $|\Delta z|/|\Delta z_M| \approx 1$). To demonstrate the sensitivity of the interferometric AFM position detector, we brought the tip in contact with a glass substrate and subsequently detached it. Due to the reduced spring constant we observed the typical jump-to-contact behavior (Figure 2B).

The vertical resolution of the AFM engine is demonstrated by sampling the surface topography of a freshly cleaved highly

oriented pyrolytic graphite (HOPG) sample (Figure 2c) using dynamic (or "tapping") mode. From the measured topography, we extracted line scans across steps of one and two atomic layers (Figure 2d), exhibiting step heights of 350 and 700 pm. These results are in good agreement with literature values of 335 pm per layer.[31] While this resolution is already sufficient for many applications, the sensitivity of the AFM position readout might be further increased by using low-noise laser sources and a Fabry–Pérot cavity with high optical Q-factor[32] rather than a simple interferometer. However, this requires highly reflective mirrors on the fiber facet and on the cantilever (see Section S5 in the Supporting Information).

3.2. Atomic Force Microscopy in Liquids

As a second example, we show the capability of our AFM engines to switch between measurements in air and in liquids, which is helpful, e.g., for imaging of biological samples,[7–9] process monitoring in chemical reactors, or for the integration of AFM engines into microfluidic systems.[33] The associated structure (**Figure 3**a) is again printed onto the facets of an SMF array, which enables remote operation over extended distances without any mechanical alignment of the AFM components. The cantilever is now designed as a massive structure with a thickness of 21 μm, leading to a dynamic behavior which is rather insensitive to the surrounding medium. Note that immersion into an ambient liquid decreases the reflection both at the SMF facet and at the curved mirror of the position detector, making the position detection more sensitive with
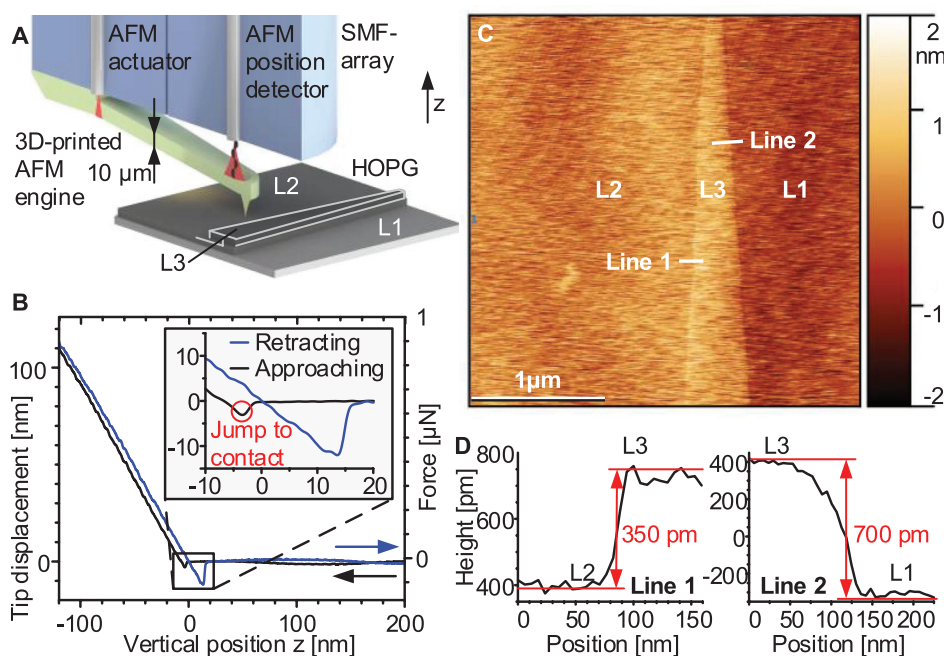

Figure 2. 3D-printed AFM engines that offers atomic step-height resolution. A) Schematic of the structure and the associated experiment, in which we sample the surface of freshly cleaved highly oriented pyrolytic graphite (HOPG). B) Characterization of the AFM position sensor. The force axis was obtained from multiplying the tip displacement with the simulated spring constant of 12. N m^{-1}. Inset: Typical jump-to-contact behavior. C) Measured surface topography of the HOPG sample. Three different atomic layers L1, L2, and L3 are visible. D) Line-scans along Line 1 and Line 2 for a one-layer (L2-L3) step and a two-layer (L3-L1) step, as indicated in C). The measured step heights amount to 350 pm for a single atomic layer and to 700 nm for two atomic layers–in agreement with literature values.[31]

ADVANCED
SCIENCE NEWS
www.advancedsciencenews.com
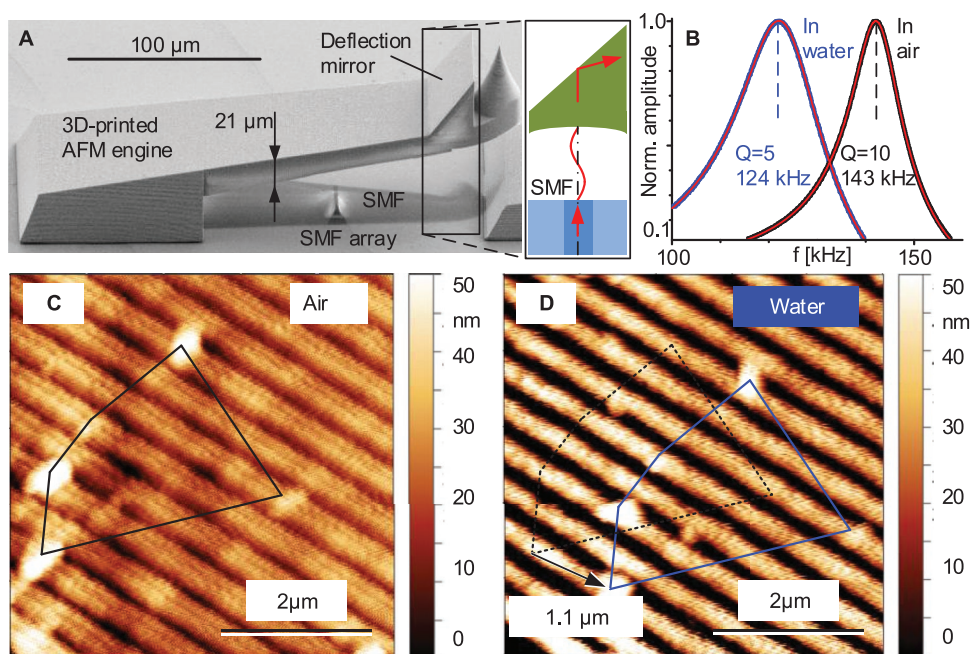
NANO · MICRO
small
www.small-journal.com

Figure 3. 3D-printed AFM engines that allow for measurements in air and in liquids. A) SEM image of the 3D-printed structure. The rather thick cantilever leads to a dynamic behavior, which is rather insensitive to the surrounding medium. Inset: To minimize the impact of spurious reflections from the sample surface, the structure is equipped with a metal deflection mirror that redirects excess light away from the optical axis of the interferometer. B) Mechanical resonance spectrum measured in air (black) and water (blue). The resonance frequency and the mechanical Q-factor were determined by a fitting a Lorentz-type model function (red) to the measured data (Section S4, Supporting Information). C,D) Surface topography of a grating structure measured in air and water without intermediate mechanical realignment of the AFM engine. The positions of surface features in air and water are indicated by black and blue lines, respectively. The two measurements show good agreement except for a minor lateral offset of 1.1 μm attributed to thermal drift of the macroscopic scan stage.

respect to spurious light reflected from the sample surface. To avoid unwanted interference, we modified the position detector by adding a metal mirror that deflects excess light away from the optical axis of the interferometer (see inset of Figure 3a). To demonstrate the performance of the system, we measured the mechanical resonance curve both in air and in water (Figure 3b). It is interesting to note that the 3D-printed SPM engines allow to locally excite the cantilever at a well-defined frequency, and that the resonance spectrum does not exhibit a "forest of peaks" as frequently observed when operating conventional AFM in liquids.[34] The ability of the presented AFM engine to subsequently work both in a liquid and in a gaseous environment without any realignment is demonstrated by sampling the same area of an optical grating with a nominal structure height of 60 nm, first in air (Figure 3c) and afterward in water (Figure 3d). Between the two measurements, we only adjusted the feedback control parameters for dynamic-mode operation and the position detector read-out wavelength to maintain an operating point of maximum sensitivity after immersing the cavity in water. The two topography measurements show a slight lateral offset of 1.1 μm, which is most likely caused by thermal drift of the macroscopic scan stage. We also observed that the measurement in air indicates a smaller height difference between the grating grooves and ribs than the measurement in water. We attribute this to a variation of the mechanical Q-factors of the cantilever when scanning in grooves compared to scanning on top of ribs. This effect is known to lead to

deviations in measured step heights.[35,36] Still, the capability of sampling nanoscopic objects in various environments without mechanical realignment of the AFM engine is a unique feature of our concept. Operation of conventional AFM assemblies in liquids typically requires mechanical realignment of the laser beam to compensate optical refraction at the liquid surface. Offering compact footprint, robustness, simple alignment, and remote operation through optical waveguides, we expect that 3D-printed SPM engines will open new perspectives for in vitro and in vivo imaging,[7–9] applications in lab-on-chip or microfluidic devices,[33] or endoscopic AFM systems.

3.3. SPM Engines for Scanning Near-Field Optical Microscopy

For standard SPM systems, co-integration with other analytical tools for multimodal sensing such as SNOM[13,14] is technically complex, often involving manual microassembly of discrete components such as metal-coated optical fibers, tuning forks, and additional optical elements for illumination or light collection. These challenges can be overcome by 3D-nanoprinting of SNOM engines as monolithic structures that comprise all relevant elements. For demonstration, we perform a first set of experiments that is dedicated to high-resolution sampling of optical fields on fiber and laser facets. To this end, we use a SNOM engine similar to the one depicted in Figure 1a, but without the tip illumination, which is not needed for
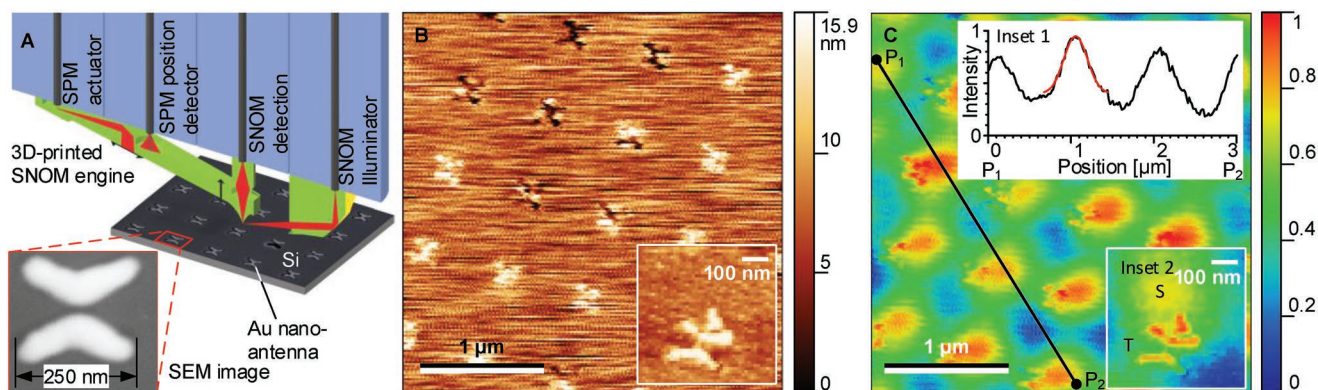
**ADVANCED
SCIENCE NEWS**

www.advancedsciencenews.com

NANO · MICRO

small

www.small-journal.com

Figure 4. Simultaneous AFM and SNOM imaging of passive optical nanostructures. A) The measurement relies on a printed AFM engine with a dedicated mirror-lens combination for local illumination of the SNOM tip (Figure 1A,B). The sample consists of metallic gold (Au) nanoantennae on a dielectric (Si) substrate. Inset: SEM image of an individual nanoantenna. B) Sample topography determined from the AFM signal. The distortions originate from the limited resolution of the large-area scanning stage (800 μm travel range) that was used in this experiment. Inset: Surface topography of an individual antenna taken with a different scanning stage. C) SNOM signal obtained when using a fiber-coupled super-continuum light source having a spectral peak at ≈1500 nm for illumination. The SNOM detector signal is normalized to the maximum value that was found in the image. Inset 1: Normalized intensity of the SNOM signal along line from P1 to P2. The resolution of the SNOM image amounts to 300 nm as indicated by the full-width at half maximum (FWHM) of a Gaussian fit (red). The performance can be greatly improved by optimizing the design and the fabrication processes. Inset 2: SNOM signal S of an individual antenna, indicating a clear topographic artefact T, which is typical for true SNOM images.[37]

characterization of active components (Section S6, Supporting Information). Building upon these results, we then demonstrate simultaneous SNOM and AFM characterization of photonic nanostructures. For these experiments, the light collection functionality is complemented by localized illumination, offered by a 3D-printed mirror-lens combination (**Figures** 1 and 4a, see also Section S1, Supporting Information). To demonstrate the functionality of the SNOM engine, we analyzed an array of gold (Au) nanoantennae on a Si-surface (Figure 4). For illumination of the SNOM tip, we use a super-continuum light source featuring a fiber-coupled power of 5 mW and a spectrum ranging from 1180 to 2400 nm with a peak around 1500 nm (Experimental Section and Section S6: Supporting Information). An SEM image of a single nanoantenna is shown in Inset of Figure 4a. Figure 4b,c shows the measured AFM topography and the corresponding SNOM image of a subsection of the antenna array. Both images were recorded simultaneously. The overview image of Figure 4b is distorted by the limited resolution of the large-area scanning stage that was used in this experiment. This problem disappears when scanning an individual antenna with a smaller scan range (Inset of Figure 4b,c). The SNOM images in Figure 4c and in the corresponding inset show some topographical artefacts, i.e., topography-induced features in the measured SNOM signal that originate from vertical movement of the aperture while scanning over the surface topography. Such topographical artefacts are typical for true SNOM images and can be avoided by measuring in so-called constant-height modus, where the tip does not follow the surface topography.[37] From the data shown in Figure 4c, we estimate a SNOM resolution of about 300 nm by fitting a Gaussian model function with a constant offset to one of the peaks and by determining the full-width at half maximum (FWHM) of the Gaussian. For an illumination wavelength of $\lambda = 1550$ nm, this corresponds to a resolution of roughly $\lambda/5$, without accounting for the finite extension of the

test structure itself, which would improve the measured resolution slightly. Please note that these experiments represent a first proof-of-concept demonstration of compact and highly scalable 3D-printed SNOM engines and that the performance of the structures has not yet been optimized. As an example, the resolution of the SNOM imaging might be improved by using, e.g., scattering-mode tips that do not feature an aperture and/or by using 3D-printed parabolic mirrors for highly efficient high-NA excitation or read-out.[29] We believe that further optimization of the design and fabrication techniques will finally enable performance parameters that are on par with highly optimized conventional SNOM systems, for which resolutions down to $\lambda/20$ were reported.[14]

4. Wafer-Level Fabrication of Arrays of SPM Engines

3D-printed SPM engines lend themselves to wafer-level mass fabrication and thus open a path toward massively parallel scanning of large sample surfaces. **Figure 5**a illustrates a vision of a SNOM array printed onto a photonic integrated circuit (PIC), instead of an SMF facet, that allows for processing of optical actuation and read-out signals. This approach allows to exploit the scalability as well as the wealth of functionalities offered by advanced photonic integration platforms such as silicon photonics,[38,39] semiconductors,[40] or low index-contrast material systems such as silicon oxide or silicon nitride.[41] Low-loss coupling between on-chip waveguides and functional part of the SPM engines can be accomplished by free-form optical coupling elements that combine, e.g., single-mode waveguides with microlenses[42] (see inset of Figure 5a).

3D-printing of advanced SPM arrays crucially relies on the reproducibility of the structures, both with respect to dimensional
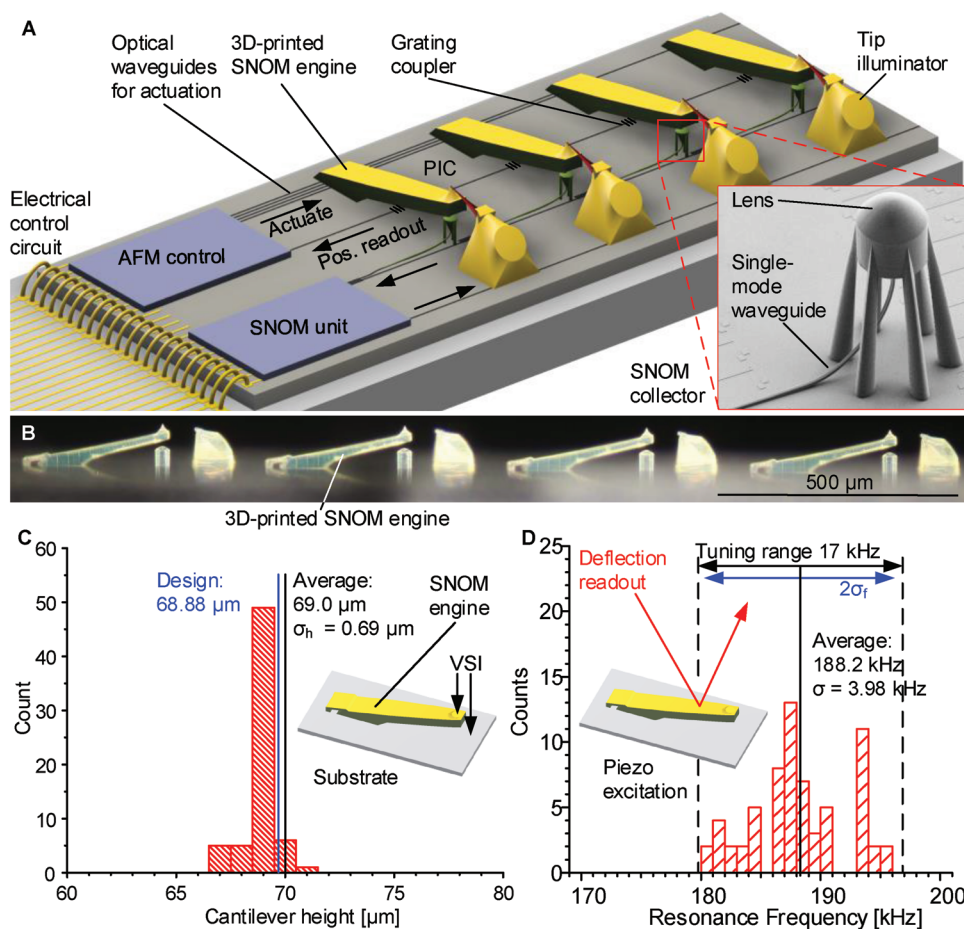
ADVANCED
SCIENCE NEWS
www.advancedsciencenews.com

NANO · MICRO
small
www.small-journal.com

Figure 5. Wafer-level fabrication and reproducibility of SPM engines. A) Vision of SPM arrays, printed onto a photonic integrated circuit (PIC) that allows for processing of optical actuation and read-out signals. Parallelization of 3D-printed SPM engines could open a path toward efficient scanning large sample surfaces. Inset: Coupling of light between SPM engines and planar lightwave circuits can either rely on grating structures,[43] as indicated for the position readout, or on free-form optical coupling elements that combine single-mode waveguides with microlenses.[42] B) Light-microscope image of four cantilevers printed on a quartz substrate. C) Histogram showing the height variation of 66 SNOM engines printed onto a plane quartz substrate. The heights exhibit a standard deviation of 690 nm. Residual height variations may be compensated using dedicated optical actuators for individual fine-tuning of the cantilever positions. D) Histogram displaying the resonance frequency of the 66 cantilevers. A piezo actuator was used to mechanically excite the cantilevers with a frequency sweep, and the readout was performed by measuring the deflection of a laser using a split photo-diode. The standard deviation amounts to $\sigma_f = 3.98$ kHz for an average resonance frequency of 188.2 kHz.

fidelity and to functional parameters such as spring constant and resonance frequency of the cantilever. To investigate these aspects, we have fabricated and characterized arrays of nominally identical SPM cantilevers on plain fused-silica substrates (Figure 5b). Results for the SNOM-type cantilever (Figure 1) are given in Figure 5c,d, whereas results for the AFM-engines (Figure 2) and details on fabrication can be found in Section S7 (Supporting Information). The reproducibility of the cantilever height above the substrate is a crucial parameter when sampling extended surfaces by a large-scale array of SPM engines. To measure the height variation, we use a vertical-scanning white-light interferometer (VSI) (Section S7, Supporting Information). A histogram of the measured height of 66 SNOM cantilevers is shown in Figure 5c, indicating a standard deviation of $\sigma_h = 690$ nm and an average height of 69 µm, i.e., a relative deviation of only 1%. The height of individual cantilevers may be controlled by using additional optical actuators for individual fine-tuning (Section S8,

Supporting Information). In addition, the reproducibility of the cantilever resonance frequency is crucial, as identical resonance frequencies allow to use a collective excitation signal for a multitude of SPM engines. The variance of the resonance frequency is measured by mechanically exciting the 66 SNOM cantilevers using a piezo actuator below the substrate and by measuring the individual oscillation amplitudes using a deflection laser. The histogram of the measured resonance frequencies is depicted in Figure 5d, indicating a standard deviation of $\sigma_f = 3.98$ kHz for an average resonance frequency of 188.2 Hz. This corresponds to a relative one-sigma uncertainty of 2.1%, which is far below the uncertainties of about 30% that are commonly reported for state-of-the-art silicon or silicon-nitride cantilevers.[10] Finally, it is interesting to note that the resonance frequency of printed SPM cantilevers can be thermally tuned by varying the average optical excitation power and hence adjusting its stiffness (Section S8, Supporting Information).

5. Conclusion and Outlook

We have introduced a novel approach for fabricating highly compact scanning probe microscopy systems with unprecedented versatility and functional design freedom. Our approach exploits high-resolution two-photon laser lithography for in situ printing of SPM engines onto the facets of optical devices, which provide optical actuation and read-out signals. Enabling high-precision monolithic co-integration of SPM engines with printed micro-optical components such as lenses and mirrors, the concept is perfectly suited for incorporating additional imaging modes such as scanning near-field optical microscopy. We demonstrate the viability of the approach in a series of experiments that range from atomic-force microscopy engines with atomic step height resolution to operation of AFM engines under water and to SNOM implementations that allow for characterizing both active and passive photonic components. We further confirm that the technique is amenable to wafer-level fabrication of massively parallel SPM arrays. Our concept may pave the path toward advanced SPM systems may unlock a wide range of scientific and industrial applications that are inaccessible to current SPM concepts.

6. Experimental Section

Fabrication of the Printed SPM Engine: A cross-section of the scanning probe microscopy engine in Figure 1a of the main manuscript is depicted in Figure S1 (Supporting Information), giving also details of the geometrical dimension. The SPM engine is printed onto the facets of an array of four single-mode fibers for near-infrared operation (AllWave FLEX, OFS, USA). The pitch of the fibers amounts to 127 µm. For printing of the SPM engine, a two-photon lithography setup is used that is based on a commercially available system (Photonic Professional GT, Nanoscribe GmbH, Germany). The machine has been extended by additional hardware features and a proprietary software package for high-precision alignment of the printed structures with respect to the fiber cores. This includes machine vision to detect the fiber facet position and tilt as well as the fiber-core position by detecting light emitted from the fiber core. As light source, a red LED was coupled into the SMF. A pulsed femtosecond laser beam is used (≈150 fs pulse duration on the sample, 80 MHz repetition rate), which is focused into the resist by a 40x-microscope objective having a numerical aperture (NA) of 1.4. The laser power is adjusted to slightly below the damage threshold of the resist. The distance of subsequent writing lines and subsequent layers to be fabricated, often referred to as "hatching and slicing distance," was set to 100 nm. The scan speed was kept at 1 mm s^{-1} at the shell of critical parts such as the tip and optically functional elements like TIR-mirrors and lenses. The cantilever itself was printed with a typical scan speed of 10 mm s^{-1}. A commercially available resist is used (IP-Dip, Nanoscribe GmbH) without applying adhesion promoter prior to fabrication. The refractive index of the exposed resist amounts to 1.53 at a wavelength[44] of 1550 nm. Further details on the fabrication of AFM tips with two-photon polymerization can be found in ref. [27]. By scanning a suitable test target, a tip radius of 25 nm could be determined here.

By applying these parameters, an RMS roughness below 40 nm is expected, which is sufficient not to degrade performance of mirror nor lenses, see ref. [24] for details on both 3D-printed lenses and mirrors.

After lithography and development, a metal cover consisting of nominally 5 nm chromium (Cr) and 100 nm gold (Au) is deposited onto the top surface of the structure using a highly directed electron-beam evaporation process in ultra-high-vacuum (UHV). A dedicated shielding structure is used to prevent unwanted coating of the lens surface that illuminates the SPM tip as well as the TIR mirror (Figure 1b). Compared to metal mirrors, TIR reflectors have a higher damage threshold and avoid undesired heating.

Atomic Step-Height Resolution: To measure the calibration curve in Figure 2b of the main manuscript, an external-cavity laser (ECL, TSL-210, Santec, USA) is used for position read-out and adjust its wavelength to one of the operating points with highest sensitivity. For small displacements Δl_C of mirror M$_I$, a linear relationship between the change of the reflected power and the mirror displacement is assumed. The proportionality factor is extracted by deforming the cantilever by bringing the tip in contact with and detached it from a hard sample surface using a closed-loop piezoelectric positioner driven by a commercially available AFM controller (ARC2, Asylum Research Inc., Oxford Instruments, UK) that comprises a signal generator for modulating the optical actuation power and a lock-in amplifier for read-out of the position detector. Here it is assumed that the incremental displacement of the tip relative to SMF array is identical to the movement of the piezo positioner and thereby allows calibrating the output signal of the position detector to the tip displacement, indicated on the vertical axis of Figure 2b. The optical signal of the position detector was received by a fiber-coupled InGaAs photodiode (PD, 2053-FC, Newport Co., USA). To avoid back-reflection from the PD an optical isolator was used. For adjusting the mechanical excitation frequency of the AFM actuator, the cantilever is first excited at its resonance and then slightly reduced the frequency such that the oscillation amplitude reduces to ≈97% of the amplitude for resonant excitation. The sample surface is then scanned in so-called dynamic mode, where the vertical position of the AFM engine is constantly adjusted such that the cantilever oscillation amplitude is kept constant. Typically, this is in the range of 60% to 90% of the free-air oscillation amplitude obtained without interaction with the sample surface. Note that for dynamic mode, the step height is deduced from the vertical position of the AFM engine and hence does not depend on the exact calibration of the cantilever position read-out. Nevertheless, the step-height resolution can be improved by increasing the sensitivity of the position read-out sensor.[32]

Scanning Near-Field Optical Microscope Measurements: The functionality of the SNOM engines was demonstrated in a series of different experiments shown in Figure 4 and Figures S7–S9 (Supporting Information). In these experiments, the same ECL and photodiodes are used as for the AFM-measurements (preceding paragraph and Section S6, Supporting Information). As samples, the facet of an SMF is used (Figure S7, Supporting Information), a semiconductor-laser (Figure S8, Supporting Information), grating couplers of a silicon photonic waveguide (Figure S9, Supporting Information), and Au-on-Si nanostructures (Figure 4). For all these samples, the topography data along with the SNOM signal was recorded.

Image and Data Processing: All SPM data was collected with Asylum Research proprietary software and processed with the freeware tool Gwyddion (http://gwyddion.net). A "polynomial fit" with degree ≤ 2 was employed, "aligned rows" and chose a suitable data range. Cross-sections of the measured data along certain lines were taken over an averaging range of ≈250 nm (Figure 2c), two lines (Figure 4c), a single line (Figure S7, Supporting Information) and 400 nm (Figure S9, Supporting Information). AFM and SNOM images were always captured simultaneously. Zoom-in data taken from the very same image (Figure S7c, Supporting Information) are indicated. All plots were created with Origin (Origin Lab Corp., USA).

Supporting Information

Supporting Information is available from the Wiley Online Library or from the author.

Acknowledgements

[1] G. Binnig, C. F. Quate, C. Gerber, *Phys. Rev. Lett.* **1986**, *56*, 930.

[2] F. J. Giessibl, *Science* **1995**, *267*, 68.

[3] S. M. Y. Sugawara, M. Ohta, H. Ueyama, *Science* **1995**, *270*, 1646.

[4] D. Pires, J. L. Hedrick, A. De Silva, J. Frommer, B. Gotsmann, H. Wolf, M. Despont, U. Duerig, A. W. Knoll, *Science* **2010**, *328*, 732.

[5] P. Vettiger, G. Cross, M. Despont, U. Drechsler, U. Dürig, B. Gotsmann, W. Haberle, M. A. Lantz, H. E. Rothuizen, R. Stutz, G. K. Binnig, *IEEE Trans. Nanotechnol.* **2002**, *1*, 39.

[6] E. Eleftheriou, T. Antonakopoulos, G. K. Binnig, G. Cherubini, M. Despont, A. Dholakia, U. Durig, M. A. Lantz, H. Pozidis, H. E. Rothuizen, P. Vettiger, *IEEE Trans. Magn.* **2003**, *39*, 938.

[7] Y. Sakiyama, A. Mazur, L. E. Kapinos, R. Y. H. Lim, *Nat. Nanotechnol.* **2016**, *11*, 719.

[8] A. P. Nievergelt, N. Banterle, S. H. Andany, P. Gönczy, G. E. Fantner, *Nat. Nanotechnol.* **2018**, *13*, 696.

[9] E. A. Lopez-Guerra, H. Shen, S. Solares, D. Shuai, *Nanoscale* **2019**, *11*, 8918.

[10] P. Eaton, P. West, *Atomic Force Microscopy*, Oxford University Press, Oxford, UK **2010**.

[11] H. P. Lang, R. Berger, C. Andreoli, J. Brugger, M. Despont, P. Vettiger, C. Gerber, J. K. Gimzewski, J. P. Ramseyer, E. Meyer, H.-J. Güntherodt, *Appl. Phys. Lett.* **1998**, *72*, 383.

[12] W. Hu, N. Anderson, Y. Qian, J. Song, J. W. Noh, S. Kim, G. P. Nordin, *Rev. Sci. Instrum.* **2009**, *80*, 085101.

[13] U. Dürig, D. W. Pohl, F. Rohner, *J. Appl. Phys.* **1986**, *59*, 3318.

[14] D. W. Pohl, W. Denk, M. Lanz, *Appl. Phys. Lett.* **1984**, *44*, 651.

[15] E. Betzig, R. J. Chichester, *Science* **1993**, *262*, 1422.

[16] R. Zhang, Y. Zhang, Z. C. Dong, S. Jiang, C. Zhang, L. G. Chen, L. Zhang, Y. Liao, J. Aizpurua, Y. Luo, J. L. Yang, J. G. Hou, *Nature* **2013**, *498*, 82.

[17] R. Hillenbrand, T. Taubner, F. Keilmann, *Nature* **2002**, *418*, 159.

[18] J. Chen, M. Badioli, P. Alonso-González, S. Thongrattanasiri, F. Huth, J. Osmond, M. Spasenovi, A. Centeno, A. Pesquera, P. Godignon, A. Z. Elorza, N. Camara, F. Javier García De Abajo, R. Hillenbrand, F. H. L. Koppens, *Nature* **2012**, *487*, 77.

[19] W. Bao, M. Melli, N. Caselli, F. Riboli, D. S. Wiersma, M. Staffaroni, H. Choo, D. F. Ogletree, S. Aloni, J. Bokor, S. Cabrini, F. Intonti, M. B. Salmeron, E. Yablonovitch, P. J. Schuck, A. Weber-Bargioni, *Science* **2012**, *338*, 1317.

[20] W. D. Herzog, M. S. Ünlü, B. B. Goldberg, G. H. Rhodes, C. Harder, *Appl. Phys. Lett.* **1998**, *68*, 688.

[21] T. Michels, V. Aksyuk, *IEEE Photonics Technol. Lett.* **2017**, *29*, 643.

[22] B. Hecht, B. Sick, U. P. Wild, V. Deckert, R. Zenobi, O. J. F. Martin, D. W. Pohl, *J. Chem. Phys.* **2000**, *112*, 7761.

[23] T. Gissibl, S. Thiele, A. Herkommer, H. Giessen, *Nat. Photonics* **2016**, *10*, 554.

[24] P.-I. Dietrich, M. Blaicher, I. Reuter, M. Billah, T. Hoose, A. Hofmann, C. Caer, R. Dangel, B. Offrein, U. Troppenz, M. Moehrle, W. Freude, C. Koos, *Nat. Photonics* **2018**, *12*, 241.

[25] N. Lindenmann, S. Dottermusch, M. L. Goedecke, T. Hoose, M. R. Billah, T. P. Onanuga, A. Hofmann, W. Freude, C. Koos, *J. Lightwave Technol.* **2015**, *33*, 755.

[26] M. R. Billah, M. Blaicher, T. Hoose, P.-I. Dietrich, P. Marin-Palomo, N. Lindenmann, A. Nesic, A. Hofmann, U. Troppenz, M. Moehrle, S. Randel, W. Freude, C. Koos, *Optica* **2018**, *5*, 876.

[27] G. Göring, P.-I. P.-I. P.-I. Dietrich, M. Blaicher, S. Sharma, J. G. J. G. J. G. Korvink, T. Schimmel, C. Koos, H. Hölscher, *Appl. Phys. Lett.* **2016**, *109*, 063101.

[28] N. Alsharif, A. Burkatovsky, C. Lissandrello, K. M. Jones, A. E. White, K. A. Brown, *Small* **2018**, *14*, 1800162.

[29] K. Edelmann, L. Gerhard, M. Winkler, L. Wilmes, V. Rai, M. Schumann, C. Kern, M. Meyer, M. Wegener, W. Wulfhekel, *Rev. Sci. Instrum.* **2018**, *89*, 123107.

[30] J. D. Adams, B. W. Erickson, J. Grossenbacher, J. Brugger, A. Nievergelt, G. E. Fantner, *Nat. Nanotechnol.* **2016**, *11*, 147.

[31] P. Trucano, R. Chen, *Nature* **1975**, *258*, 136.

[32] H. I. Rasool, P. R. Wilkinson, A. Z. Stieg, J. K. Gimzewski, *Rev. Sci. Instrum.* **2010**, *81*, 023703.

[33] K. Schoenwald, Z. C. Peng, D. Noga, S. R. Qiu, T. Sulchek, *Rev. Sci. Instrum.* **2010**, *81*, 053704.

[34] T. E. Schäffer, J. P. Cleveland, F. Ohnesorge, D. A. Walters, P. K. Hansma, *J. Appl. Phys.* **1996**, *80*, 3622.

[35] D. Ebeling, H. Hölscher, H. Fuchs, B. Anczykowski, U. D. Schwarz, *Nanotechnology* **2006**, *17*, S221.

[36] H. Hölscher, U. D. Schwarz, *Appl. Phys. Lett.* **2006**, *89*, 073117.

[37] B. Hecht, H. Bielefeldt, Y. Inouye, D. W. Pohl, L. Novotny, *J. Appl. Phys.* **1998**, *81*, 2492.

[38] A. H. Atabaki, S. Moazeni, F. Pavanello, H. Gevorgyan, J. Notaros, L. Alloatti, M. T. Wade, C. Sun, S. A. Kruger, H. Meng, K. Al Qubaisi, I. Wang, B. Zhang, A. Khilo, C. V. Baiocco, M. A. Popović, V. M. Stojanović, R. J. Ram, *Nature* **2018**, *556*, 349.

[39] J. Wang, S. Paesani, Y. Ding, R. Santagati, P. Skrzypczyk, A. Salavrakos, J. Tura, R. Augusiak, L. Mančinska, D. Bacco, D. Bonneau, J. W. Silverstone, Q. Gong, A. Acín, K. Rottwitt, L. K. Oxenløwe, J. L. O'Brien, A. Laing, M. G. Thompson, *Science* **2018**, *360*, 285.

[40] F. Kish, V. Lal, P. Evans, S. W. Corzine, M. Ziari, T. Butrie, M. Reffle, H.-S. Tsai, A. Dentai, J. Pleumeekers, M. Missey, M. Fisher,

ADVANCED
SCIENCE NEWS

www.advancedsciencenews.com

NANO · MICRO

small
www.small-journal.com

S. Murthy, R. Salvatore, P. Samra, S. Demars, N. Kim, A. James, A. Hosseini, P. Studenkov, M. Lauermann, R. Going, M. Lu, J. Zhang, J. Tang, J. Bostak, T. Vallaitis, M. Kuntz, D. Pavinski, A. Karanicolas, B. Behnia, D. Engel, O. Khayam, N. Modi, M. R. Chitgarha, P. Mertz, W. Ko, R. Maher, J. Osenbach, J. T. Rahn, H. Sun, K.-T. Wu, M. Mitchell, D. Welch, *IEEE J. Sel. Top. Quantum Electron.* **2018**, *24*, 1.

[41] K. Y. Yang, D. Y. Oh, S. H. Lee, Q.-F. Yang, X. Yi, B. Shen, H. Wang, K. Vahala, *Nat. Photonics* **2018**, *12*, 297.

[42] M. Blaicher, M. R. Billah, T. Hoose, P.-I. Dietrich, A. Hofmann, S. Randel, W. Freude, C. Koos, A. Hofmann, S. Randel, W. Freude, C. Koos, C. Koos, in *Conf. Lasers Electro-Optics*, OSA, San Jose, CA, USA **2018**, p. STh1A.1.

[43] D. Taillaert, W. Bogaerts, P. Bienstman, T. F. Krauss, P. Van Daele, I. Moerman, S. Verstuyft, K. De Mesel, R. Baets, *IEEE J. Quantum Electron.* **2002**, *38*, 949.

[44] S. Dottermusch, D. Busko, M. Langenhorst, U. W. Paetzold, B. S. Richards, *Opt. Lett.* **2019**, *44*, 29.

1904695 (10 of 10)